ACS APPLIED MATERIALS & INTERFACES

www.acsami.org

Research Article

Biocompatible All-in-One Adhesive Needle-Free Cup Patch for Enhancing Transdermal Drug Delivery

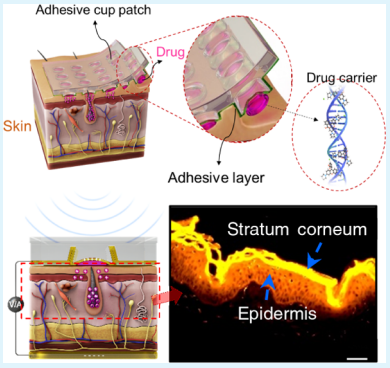
Moonjeong Bok, Zhi-Jun Zhao, Soon Hyoung Hwang, Yongrok Jeong, Jiwoo Ko, Junseong Ahn, Ju Ho Lee, Sohee Jeon, and Jun-Ho Jeong*

Cite This: *ACS Appl. Mater. Interfaces* 2021, 13, 58220–58228

Read Online

ACCESS | Metrics & More | Article Recommendations | Supporting Information

ABSTRACT: Patch-type drug delivery has garnered increased attention as an attractive alternative to the existing drug delivery techniques. Thus far, needle phobia and efficient drug delivery remain huge challenges. To address the issue of needle phobia and enhance drug delivery, we developed a needle-free and self-adhesive microcup patch that can be loaded with an ultrathin salmon DNA (SDNA) drug carrier film. This physically integrated system can facilitate efficient skin penetration of drugs loaded into the microcup patch. The system consists of three main components, namely, a cup that acts as a drug reservoir, an adhesive system that attaches the patch to the skin, and physical stimulants that can be used to increase the efficiency of drug delivery. In addition, an ultrathin SDNA/drug film allows the retention of the drug in the cup and its efficient release by dissolution in the presence of moisture. This latter feature has been validated using gelatin as a skin mimic. The cup design itself has been validated by comparing its deformation and displacement with those of a cylindrical structure. Integration of the self-adhesive microcup patch with both ultrasonic waves and an electric current allows the model drug to penetrate the stratum corneum of the skin barrier and the whole epidermis, thereby enhancing transdermal drug delivery and reducing skin irritation. This system can be used as a wearable biomedical device for efficient transdermal and needle-free drug delivery.



KEYWORDS: *self-adhesive, microcup patch, needle phobia, transdermal drug delivery, drug carrier, effective delivery*

1. INTRODUCTION

Recently, with the spread of the coronavirus disease 2019 (COVID-19) global pandemic, the topic of vaccine injections has attracted increased attention.[1−5] Currently, vaccines are administered using a syringe with a sharp solid needle.[6,7] However, it has been reported that at least 10% of the world's population suffer from severe needle phobia, hindering their ability to receive vaccines or other drugs.[8] It is, therefore, very important to overcome the challenge of needle phobia. One attractive solution is the minimally invasive intradermal approach, which allows drugs to be delivered through the skin without a needle, referred to as a transdermal delivery system. Unlike subcutaneous injections that cause pain and bleeding, it has the advantages of being sustained, painless, and self-administrable, while being easy to use. The existing transdermal patches[9−15] (i.e., matrix patches, reservoir patches, microneedle patches) are attached to the skin using an adhesive tape to achieve drug delivery. The active ingredient is delivered via the transdermal route, through the stratum corneum, the outermost layer that protects the skin and inhibits drug absorption. It is, therefore, important that the drug crosses the superficial skin barrier, avoiding contact with the critical nerves and capillaries of the epidermis.

Currently, research on dissolving microneedles in the human body is attracting attention. In the case of dissolving microneedles, the mechanical properties of the material that facilitate penetration into the skin barrier for stable drug delivery and conformal attachment on the skin for ideal penetration and fixation are considered. However, some substances do not penetrate the skin evenly and dissolve quickly; thus, they cannot be delivered easily. Moreover, there are restrictions on the adhesion of the substances to the skin except for the needles used to deliver the drug.[16,17]

For example, hydrophilic, charged, or large molecules, such as various biological drugs (proteins, peptides, genetic materials), have difficulty in passing through the stratum corneum of the skin.[18,19] Therefore, for flexible and efficient drug delivery, research is also underway to deliver therapeutic drugs into the body by triggering drugs through various approaches (e.g., magnetic fields, ultrasound, electric fields).[20−23] In addition to improving drug delivery, their effectiveness, expandability, convenience, compatibility with skin, and adhesive abilities should be addressed when

Received: September 28, 2021
Accepted: November 8, 2021
Published: November 18, 2021



Downloaded via KOREA ADVANCED INST SCI AND TECHLGY on November 21, 2022 at 13:58:25 (UTC).
See https://pubs.acs.org/sharingguidelines for options on how to legitimately share published articles.

ACS Publications

© 2021 American Chemical Society

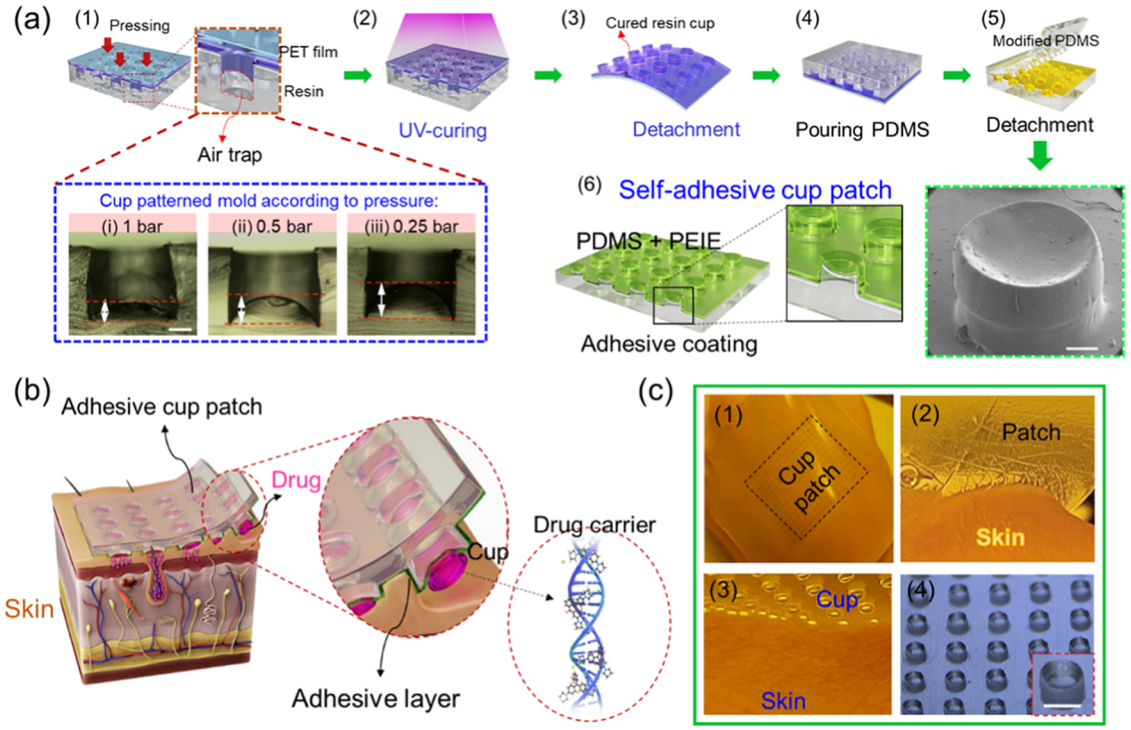


Figure 1. (a) Fabrication process used for self-adhesive cup patches. (1) Apply pressure after equilibration of the resin solution (the enlarged image shows the change in the depth of the cup structure using pressure of different magnitudes: (i) 1 bar, (ii) 0.5 bar, (iii) 0.25 bar; scale bar: 200 μm). (2) UV irradiation of the resin solution. (3) Peel off the poly(ethylene terephthalate) (PET) film after curing to confirm the formation of the cup structure. (4) Pour PDMS onto the resin cup film, cure, and peel off. (5) Chemically coat for easy separation and pour modified PDMS, cure, and peel off. (6) Apply adhesive material for adhesion. The dotted line indicates a focused ion beam (FIB) image of the cup structure in the cup patch (scale bar: 200 μm). (b) Schematic illustration of the self-adhesive microcup patch. The enlarged circles with dotted lines provide a close-up view of the adhesive layer and the microcups as well as a drug carrier with salmon DNA (SDNA) molecules as a biomaterial. (c) Image of the actual cup patch. (1) Image of cup patch attached to the back of the hand. (2, 3) Image after peeling the cup patch off the skin. (4) Optical image of the cup structure in the patch (scale bar: 1 mm).

developing drug delivery patches. These patches have a wide range of applications in tissue repair and regeneration, and they play an important role in clinical medicine. Therefore, it is necessary to consider the adhesion of the drug delivery system to the biological interface, which is the skin.[17,24,25] Thus far, existing patches have achieved attachment to the skin through tape fabricated onto the side of the patches, leading to imperfect contact between integral patches and skin, thereby affecting drug delivery.

To achieve painless drug delivery and full contact between patches and skin, a self-adhesive microcup patch as a drug carrier and an ultrathin salmon DNA (SDNA) drug film were developed to improve patch adhesivity, overcome needle phobia, and improve drug delivery. SDNA with excellent biocompatibility and biodegradability has been used as a raw material for clinical treatment. This material has advantages that can help to repair skin and regenerate cartilage, which can also be used as a template for hosting various functional substances, such as proteins and drugs.[14,26−29] Therefore, in the present study, the biocompatible SDNA film was used to maintain the stability of drug loading in the adhesive cup patches. In addition, a gel containing moisture, as an experimental skin, was used to evaluate the performance of the microcup patches in delivering a drug. Pigskin was used to explore the ability of the microcup patches to deliver drugs by penetrating the skin, and a combination of ultrasonic sound and electric current as physical stimulators was also implemented to increase drug release effectively. We believe, microcup patch will be an important help in future drug delivery.

2. RESULTS AND DISCUSSION

Figure 1a illustrates the process used to fabricate the microcup patch. The process is divided into two stages, namely, fabrication of the resin cups and fabrication of the adhesive microcup patch. A detailed explanation is provided in Section 4 and Figure S1. To obtain the cup from the poly(dimethylsiloxane) (PDMS) mold with holes, the meniscus and air trap phenomenon was used to achieve the cup shape by controlling the UV curing time and pressure, thereby, obtaining a mold with a cup structure (Figure 1a1−3). A similar method was reported by Baik et al.[30,31] During the fabrication process, the curvature of the cup was adjusted by changing the pressure (Figure 1a1, inset). To achieve the final cup design, different pressures (1, 0.5, and 0.25 bar) were used in the fabrication of the cup-shaped mold. From the data shown in Figure 1a1i−iii, it is observed that as the pressure decreased, the curvature increased. This is because when a small pressure is applied, the large volume of trapped air prevents the resin solution from filling the holes of the mold, thus, resulting in a resin mold with a larger curvature. The curvature of the microcup is important for drug delivery, because as the curvature increases, the volume of the cup increases, which allows the drug to be stably stored in the cup. In other words, the cup structure in the proposed patch is a space for temporary drug storage. Therefore, since a large-

https://doi.org/10.1021/acsami.1c18750
ACS Appl. Mater. Interfaces 2021, 13, 58220−58228

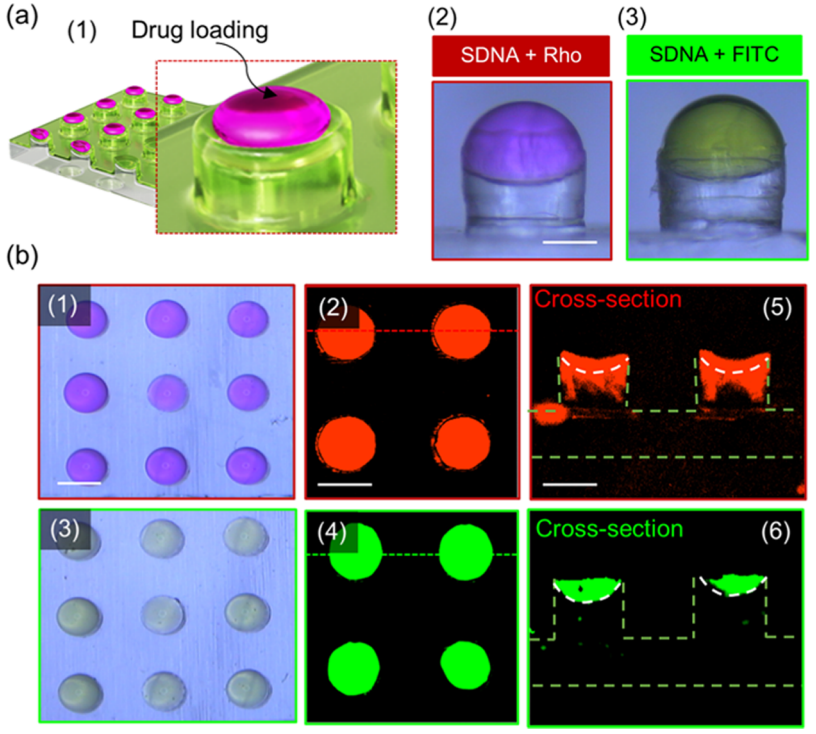


Figure 2. (a) (1) Schematic illustration of the drug-loaded cup patches. The enlarged dotted square shows the SDNA/fluorescent dye solution (rhodamine B (Rho) or FITC−dextran (FITC)) loaded into a cup. Side images of the cup loaded with (2) a solution containing a mixture of SDNA and Rho (scale bar: 500 μm) or (3) a solution containing a mixture of SDNA and FITC. (b) Top-view images of the drug-loaded cups. (1, 3) Optical image of 3 × 3 cups loaded with a mixture of SDNA/Rho and SDNA/FITC, respectively. (2, 4) Fluorescent images of 2 × 2 cups loaded with SDNA/Rho and SDNA/FITC, respectively. (5, 6) Fluorescent side images (cross sections) of two cups loaded with SDNA/Rho and SDNA/FITC, respectively (scale bar: 1 mm).

volume cup capable of stably loading and storing drug would be ideal, a microcup patch for drug delivery was manufactured by selecting the lowest pressure possible, which was 0.25 bar.

The fabricated resin cup was then used as a master to obtain a flexible and attachable microcup patch. A PDMS mold of the designed cup was replicated from the resin cup master, as shown in Figure 1a4. Following this, a chemical coating layer was added to enable easy separation from the PDMS cup mold as shown in Figure 1a5. The modified PDMS with a mixture of Sylgard 184, Sylgard 527, and polyethylenimine (PEIE) was fabricated into a microcup patch that could be repeatedly replicated from the PDMS cup mold, as shown in Figure 1a5. The modified PDMS imparts the microcup patch with a self-adhesive property.[32,33] Finally, the adhesive materials with a constant weight percentage of PDMS and PEIE[33] were coated onto the surface of the fabricated microcup patches, forming the self-adhesive microcup patches (Figure 1a6).

Figure 1b shows a schematic of a microcup-containing patch attached to the skin. The microcup patch consisted of an adhesive patch for skin attachment and a microcup that could be loaded with a drug to act as a drug reservoir, as shown in Figure 1b. These reservoirs provide a well-controlled environment for different drug formulations allowing for the control of drug stability and timing of drug delivery. For stable loading of the drug into the microcup patch, biocompatible SDNA was used as a drug carrier. When the microcup patch was attached to the surface of the moisturized skin, the drug carrier was transferred onto the surface of the skin from the microcup patch owing to its solubility. Subsequently, the drug penetrated the skin along a concentration gradient. Figure 1c1−3 shows the attachment and detachment of a microcup patch from hand skin. It was confirmed that the microcup patch had good skin-adhesion properties. An optical image of the well-arranged microcup patch is shown in Figure 1c4.

To evaluate the drug loading and highlight that a cup patch can contain a variety of drugs and that the different drugs can be easily loaded in each cup, rhodamine B (Rho) and fluorescein isothiocyanate (FITC)−dextran (FITC), as two model drugs, were mixed with SDNA solution as a drug carrier. The SDNA plays an important role by forming a film that essentially fixes the drug (Figure 3a). Figure 2 shows images of the model drugs (SDNA−rhodamine B and SDNA−FITC) loaded into the cups of the self-adhesive microcup patches. Figure 2a2,3 shows optical images of SDNA−rhodamine B and SDNA−FITC, loaded into the microcup. Figure 2b shows optical and fluorescent top-views and fluorescent cross-sectional views of cups containing the two types of model drugs. The images provide strong evidence that the drug models could be efficiently loaded onto the microcup patches. Our method allows not only the maintenance of the drug in the cup but also easy loading of different drugs in each cup and control the amount of drug depending on the requirements.

Figure 3 elucidates the structural properties of the microcup and the role of SDNA. To characterize the microcup structure, we compared it with a cylindrical structure. In the case of the cylindrical structure (Figure 3a2), although the drug carrier film (SDNA/drug film) could be fabricated, the drug film was not uniformly coated on the cylinder with the adhesive material. In addition, when the drug was loaded into the microcup without SDNA, the drug became concentrated along the side of the cup, and the distribution was uneven (Figure 3a3). The schematic and FIB images are shown in Figure 3. A

https://doi.org/10.1021/acsami.1c18750
ACS Appl. Mater. Interfaces 2021, 13, 58220−58228

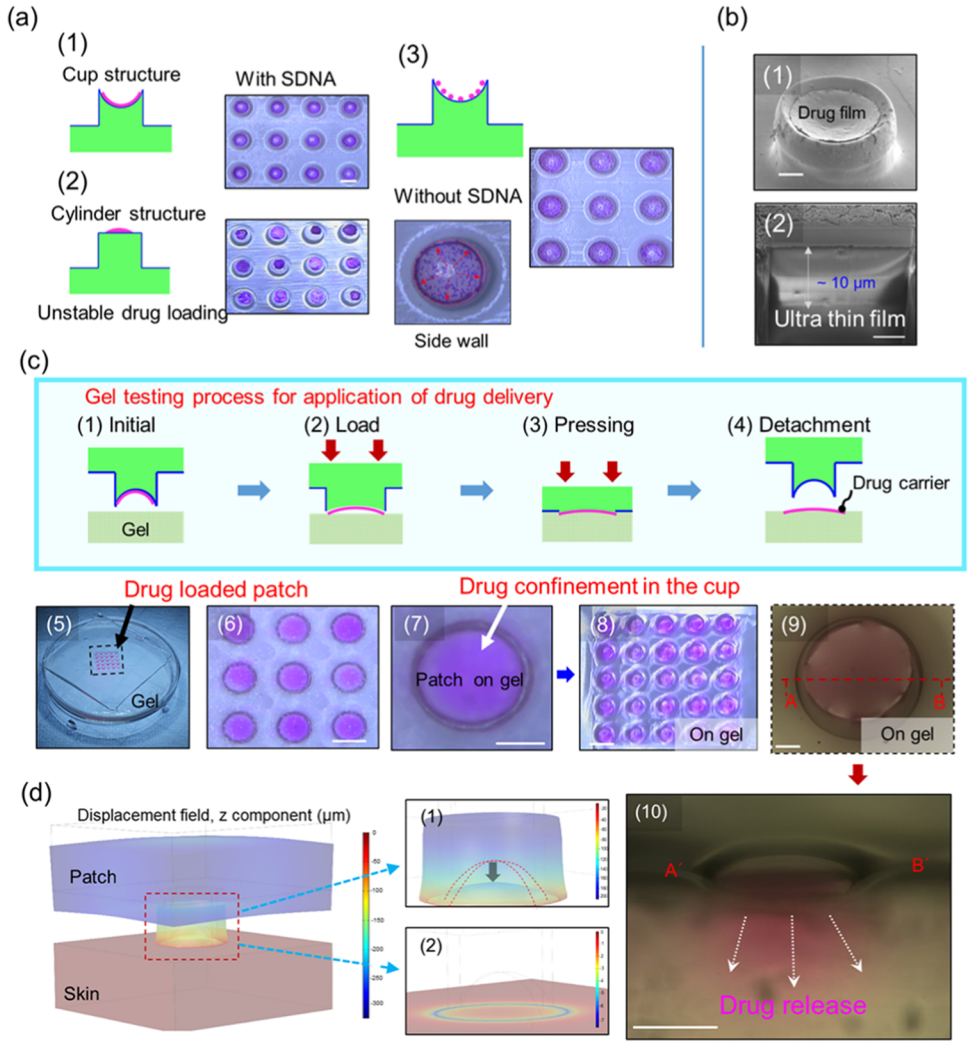


Figure 3. (a) Validation of the structure of the microcup and the use of SDNA. (1) Drug films loaded into the microcups. (2) Drug films loaded into a cylinder structure. (3) Drug loading into microcups in the absence of SDNA (scale bar: 1 mm). (b) Focused ion beam (FIB) images of (1) a cup containing a drug film and (2) thickness of the fabricated drug film (scale bars: (1) = 200 μm and (2) = 5 μm). (c) Schematic diagram of the gel testing process used to assess the use of the drug-loaded microcup patches for drug delivery. (1) Before patch attachment (Initial). (2) During attachment (Load). (3) Attachment state (Pressing). (4) Drug delivery onto the gel after patch detachment (Detachment). (5) Actual image of the cup patch on the gel. (6) Enlarged top-view image of 3 × 3 cups (scale bar: 1 mm). (7) Top-view image of one cup showing confinement of the drug to the cup (scale bar: 500 μm). (8) Top-view image of the gel after patch detachment (scale bar: 1 mm). (9) Enlarged image (scale bar: 200 μm). (10) Cross-sectional image showing the release of the drug from the gel (scale bar: 500 μm). (d) Displacement field simulation of the cup patch/skin. (1) Cup portion. (2) Skin portion.

drug carrier film with an ultrathin thickness of 10 μm was observed, as shown in Figure 3b1,2. In the cup patch, it is important to ensure that the drug film in the manufactured patch is in contact with the surface, and the drug film in the fabricated patch is maintained efficiently (Figure S5b,c). Therefore, in Figure 3c, delivery of dissolution and stable drug film was demonstrated using gelatin, a phantom tissue that mimicked skin tissue and possessed even moisture distribution. Figure 3c1−4 shows the process used to assess dissolution onto gelatin. First, self-adhesive microcup patches loaded with drug carrier film were attached to the surface of the gelatin (Figure 3c1−3). As a result, the film on the cup was transferred onto the surface of gelatin owing to the moisture of the gel (Figure 3c4). Figure 3c5−7 shows images of the drug carrier film containing the microcup patch attached to the gelatin, and the related top-view images are shown in Figure 3c6,7. As shown in Figure 3c8,9, the drug film was successfully transferred onto the surface of gelatin. In addition, after the transfer, the drug film gradually penetrated the interior of the gelatin. This is because the moisture in the gelatin dissolves the drug carrier film, thereby allowing for drug delivery, as shown in Figure 3c10. To observe the skin deformation that occurred when the self-adhesive microcup patch was attached to the skin, a structural simulation was performed using COMSOL Multiphysics. Figure 3d shows the simulation results when the self-adhesive microcup patch was attached to the surface of the skin. When a load was applied to the elastic cup structure, the surface area increased, and stress deformation occurred on the side of the cup as opposed to along the cylindrical surface (Figure S4). Figure 3d1,2 shows that the deformation of the self-adhesive microcup patch and skin corroborated with the experimental data observed in the gelatin test.

After the preliminary test, in vitro drug delivery to pigskin was assessed using the self-adhesive microcup patch. To

https://doi.org/10.1021/acsami.1c18750
ACS Appl. Mater. Interfaces 2021, 13, 58220−58228

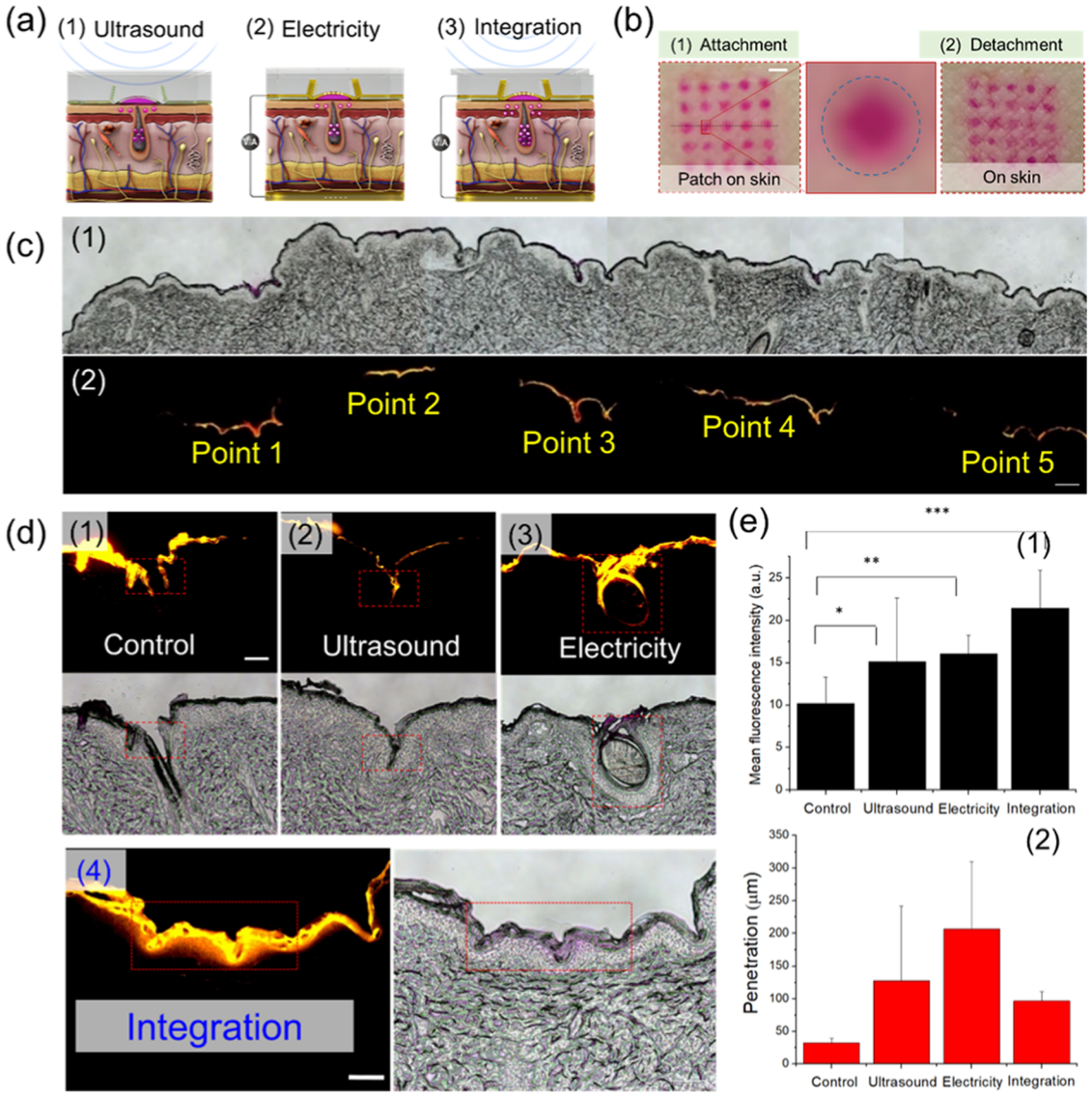


Figure 4. Combination of the drug-loaded microcup patch with physical enhancers to trigger drug release into the skin. (a) Schematic diagram showing (1) ultrasound, (2) electricity, and (3) the combination of ultrasound and electricity (integration). (b) (1) Top-view image of a drug-loaded cup patch applied to pigskin. (2) Top-view image after peeling the microcup patch off. The dotted circle shows that the drug slowly dissolves in the cup (scale bar: 2 mm). (c) Cross-sectional views of pigskin after loading the drug using continuous five cups. (1) Optical image. (2) Fluorescent image (scale bar: 100 μm). (d) Fluorescent and optical images of pigskin after applying different physical enhancers for 30 min. (1) Control, (2) ultrasound, (3) electricity, (4) integration (scale bar: 100 μm). (e) (1) Comparison of the mean fluorescence intensity for each group quantitated using ImageJ. (2) Comparison of the penetration depth for each group quantitated using ImageJ; * indicates statistical significance compared to the "control" group at a P-value of <0.05 using the Student's t-test; n = 5/group.

physically stimulate drug delivery from the microcup patch, rather than relying on simple diffusion, skin sections with the attached microcup patch were exposed to ultrasound, electrical current, and the combination of the two. Figure 4a shows a schematic of the drug delivery process including the additional physical stimulators. It is well known that exposure to ultrasound can improve the diffusivity of the stratum corneum via mechanical vibrations at a constant frequency. Electric current can improve drug permeability of the skin by the repulsion of ionic drugs when a potential difference is applied to the skin.[23,34,35] A combination of the two physical approaches may further enhance drug delivery. Rhodamine B, which is hydrophilic and positively charged, was used as a model drug to assess skin penetration. Self-adhesive microcup patches loaded with the SDNA/rhodamine B drug film were first attached to the surface of the pigskin. Images of the attachment and detachment processes are shown in Figure 4b1,2. The drug film was trapped inside the cup structure, and the film slowly dissolved because of the moisture present on the skin surface. When the patch was removed after 30 min, the drug film present in the microcup had dissolved and moved to the skin surface, as shown in Figure 4b2. The skin was exposed to three different physical stimulants as described above for 30 min each, after which cryo-blocks of the skin were prepared and frozen sections were made to test for the successful delivery of rhodamine B. The extent of skin penetration of rhodamine B resulting from these three different physical stimulants was compared to the skin penetration obtained using a simple concentration gradient as a control. Figure 4c1,2 shows the optical and fluorescent cross-sectional

https://doi.org/10.1021/acsami.1c18750
ACS Appl. Mater. Interfaces 2021, 13, 58220−58228

images of the skin beneath by five adjacent microcups. Figure 4d (refer to Figure S7) shows cross-sectional images of the skin exposed to the three physical stimulants to trigger drug release into the skin. Although the model drug, hydrophilic rhodamine B, has a molecular weight of about 500 Da, it is somewhat difficult to diffuse it into the skin through a simple concentration gradient. The reason is that the outermost layer of the skin, the stratum corneum, has low water permeability; therefore, in the case of hydrophilic substances, even if the molecular weight is low, drug delivery is limited. However, its penetration into the skin pores following exposure to ultrasound and electric current, respectively, were clearly observed. In the case of the control, rhodamine B fluorescence was observed only in the stratum corneum and the upper part of the hair in the pore area (Figures 4d1 and S7.1). In the case of ultrasound and electric current exposure, a fluorescence signal was observed in the stratum corneum and under the hair in the pore area (Figures 4d2,3, S7.2, and S7.3). Therefore, when a physical stimulator was used alone, drugs were loaded so that they could penetrate sufficiently through the hair follicle, an appendage of the skin, for drug delivery. Here, the penetration depth indicated the hair follicle area. Interestingly, when ultrasound and electric current were combined (integration) (in Figures 4d4 and S7.4), rhodamine B was delivered to the epidermis. The mean fluorescence intensity increased by about 2.2 folds when both ultrasound and electric current were used with the microcup patch compared to the patch alone (Figure 4e1). In addition, in the case of the integrated system, the mean fluorescence signal intensity showed the maximum value, but the penetration depth was lower than that of ultrasound or electric current alone. A low penetration depth was expected for an integrated system because it shows absorption of rhodamine B over a large area. In other words, for a single system (ultrasound only, or electric current only), drugs were delivered through the skin appendages, and for the integration, drugs were delivered to the epidermis across the stratum corneum barrier. In the case of the integrated system, combined with the increased diffusivity into the stratum corneum induced by ultrasound and the electroosmotic effect induced by the electric current, the function of the intrinsic skin barrier was altered. Therefore, we have demonstrated the potential to accelerate transdermal delivery. The microcup patch developed in this study has potential applications for the local anesthetic lidocaine,[36] various vaccines,[37,38] and other drugs that are typically administered using microneedles[39,40] and is expected to be effective in drug delivery as a user-friendly all-in-one drug patch in the future. Thus, the self-adhesive microcup patch could be an efficient wearable biomedical drug delivery platform, which not only addresses the challenge of needle phobia but can also be self-administered in a facile manner.

3. CONCLUSIONS

In summary, we developed an all-in-one self-adhesive, needle-free, microcup patch that can conveniently and effectively enhance the delivery of any drug loaded into the microcup. In addition, an excellent drug delivery carrier was prepared by mixing a solution of the drug and SDNA. This approach can be used to reliably load and retain the drug in the cup. The microcup patch showed strong adhesion and ease of detachment to the skin mimic. The efficacy of the self-adhesive microcup patch loaded with an SDNA drug film was assessed in vitro using pigskin. The effect of physical stimulants, such as ultrasound, electric current, and a combination of both, was also assessed. The combination of ultrasound and electric current enhanced the performance of the self-adhesive microcup patch, allowing the drug to penetrate the epidermis. This self-adhesive microcup patch system may be useful for simplifying drug administration to patients. The extent of drug penetration can be controlled through modification with physical stimulants. This system can be used as an efficient wearable biomedical device for drug delivery.

4. EXPERIMENTAL PROCEDURE

4.1. Fabrication of the Self-Adhesive Microcup Patch. *4.1.1. Microcup Structured RM-311/PET Film.* For patterning of the microcup structures, we referred to the method previously described by Baik et al.[30,31] To pattern the microcup structure on the prepared PDMS hole-patterned mold, we took advantage of the meniscus phenomenon. Trichloro(1*H*,1*H*,2*H*,2*H*-perfluorooctyl)-silane (FOTCS; Sigma-Aldrich, Korea), which can form an antiadhesion self-assembled monolayer, and the prepared PDMS mold were placed in a Teflon box and incubated in an oven at 80 °C for 30 min. This was performed because the diameter and depth of the periodic holes were large, making it difficult to form a meniscus. The FOTCS-treated PDMS mold was then placed on the underside of a press machine, and RM-311 resin (Minuta Technology Co., Ltd., Korea; polyurethane) was drop-cast onto the PDMS mold, after which it was slowly covered with a PET film (polyethylene terephthalate; thickness: 1 mm) (Figure S1f).

After exposing the solution to the atmosphere for 3 min to equilibrate the holes, the RM-311 resin and the hole pattern mold were uniformly compressed for 1 min at a pressure of 0.25 bar (Figure 1a1). Subsequently, the pressing surface was irradiated for 100 s with ultraviolet rays. The PET film of the cured RM-311 microcup structure was then peeled off from the PDMS mold, and the peeled film was irradiated with ultraviolet rays for 20 min further to allow for complete curing (Figure 1a2,3).

4.1.2. Fabrication of the Self-Adhesive Microcup Patch. The prepared cup-structured RM/PET film was attached to a Petri dish, and PDMS, prepared by mixing the elastomer and a curing agent at a 10:1 ratio, was poured onto the RM cup structure (Figure 1a4). After pouring, vacuum treatment was performed for 15 min to remove air bubbles, and the PDMS was cured at 75 °C for 90 min. Subsequently, the PDMS mold was gently separated from the RM cup structure. As the PDMS must be poured again onto the separated PDMS mold to make a patch, it was spin-coated at 4000 rpm for 45 s with the polymer 495 PMMA A4 solution (MicroChem) to allow easy separation from the separated PDMS mold (Figure 1a5). After coating, the mixture was baked at 180 °C for 2 min. Thereafter, 10 g of PDMS 184 elastomer and a curing agent at a 10:1 weight ratio, 10 g of PDMS 527 elastomer and curing agent at a weight ratio of 1:1,[32] and 60 μL of PEIE solution (Sigma-Aldrich, Korea; polyethylenimine, 80% ethoxylated solution) were mixed and molded again (Figure 1a5). The curing temperature was 80 °C. After curing, to allow the cup-structured patch to adhere to the skin, 40 μL of PEIE[33] was mixed with PDMS 184 (10:1 ratio, 10 g) (Figure 1a6) and spin-coated onto the patch at 5000 rpm for 60 s. The curing temperature was maintained at 80 °C.

4.2. Peel Test. To perform a peel test, a pigskin sample was fixed to a lower plate. The adhesive patch was attached to the skin and then fixed to an upper clamp. When the upper clamp was raised at a constant speed, a load cell measured the force required to peel the patch off the pigskin. The average peel strength was calculated by measuring the average load of the peel test and dividing it by the attachment area (area: 112 mm^2).

4.3. Preparation of SDNA. *4.3.1. Preparation of SDNA Solution Embedded with Rhodamine B or FITC–Dextran.* SDNA (0.1 g, HTL Biotechnology, France; highly polymerized deoxyribonucleotides, sodium salt—low molecular weight—medical-grade, extracted from salmon milt) was dissolved in 10 mL of deionized water to prepare a 1 wt % SDNA solution. The solution was stirred using a

https://doi.org/10.1021/acsami.1c18750
ACS Appl. Mater. Interfaces 2021, 13, 58220−58228

magnetic bar for 5 h at approximately 500 rpm at room temperature to obtain a homogeneous mixture of DNA and rhodamine B (0.0025 g; Sigma-Aldrich, Korea; for fluorescence molecular weight 479.01) or FITC−dextran (0.0025 g; Sigma-Aldrich, Korea; fluorescein isothiocyanate−dextran, average molecular weight 70 000).

4.4. Fabrication of the DNA Film Embedded with Rhodamine B. The SDNA/rhodamine B solution was dispensed into the microcup patch with a 1 μL micropipette. After dispensing, the microcup patch was heated at approximately 50 °C for 5 min to prepare the microcup loaded with the SDNA/rhodamine B film.

4.5. Gel Test of Film Transfer. Gelatin hydrogel (Sigma-Aldrich, Korea; gel strength ∼300 g Bloom, Type A) extracted from porcine skin was used to show the effectiveness of the SDNA film in the patch, for drug delivery. A 20 wt % gelatin solution was placed in a Petri dish and left at room temperature for 30 min for gelation. After gelation, the patches were attached to the gel. It was confirmed that the SDNA film in the patches was transferred to the gel surface.

4.6. Physical Stimulants. For ultrasonic stimulation, a commercial product (Ahrong Eltech, Korea, Rex-kara) that generates 1.7 million micro-vibrations per second was used. After enough gel was applied to the patch, the ultrasonic device was applied.[23] For electrical stimulation, a power supply was used as the electrical source, metal was deposited on the cup patch as the anode, and aluminum foil under the skin was used as the cathode. For skin attachment, an adhesive layer was coated around the cup in the patch, except for the electrode wire part. The applied area was approximately 16 cm^2, and the skin thickness was approximately 5 mm as whole skin. The applied voltage and current were DC 6V and <0.18 mA/cm^2. In the case of an integrated system, both were applied. Each experiment was treated the same for 30 min.

4.7. Fluorescence Microscope Imaging. The thickness of porcine cadaver skin used in this study was approximately 5 mm (Medi Kinetics Micro-pig, Pyeongtaek, Korea). All skin samples were stored at 4 °C until testing. This study was approved by the Institutional Animal Care and Use Committee. The penetration of the fluorescent substance rhodamine into the in vitro skin sample was assessed after allowing for simple diffusion, after ultrasonic treatment, after application of an electric current, or after a combination of ultrasonic treatment with electric current. The exposed surface of the skin was examined under a microscope to analyze the depth of penetration. The porcine cadaver skin samples were frozen using a freezing block and then cut into 10 μm sections in the z-axis direction to create frozen sections. Cross sections of these sections were visualized using the 10× objective lens of a fluorescence microscope. To compare the quantified average fluorescence signal intensity using ImageJ, the images at the same magnification and in the same area were used to obtain the average fluorescence signal intensity. The penetration depth also was measured using the same program.

4.8. Statistical Analysis. Results are expressed as mean ± standard deviation. All statistical data were analyzed using the Student's t-test. In all cases, statistical significance was set at $P \leq 0.01$.

4.9. Simulation. The solid mechanics module of the COMSOL Multiphysics software (www.comsol.com) was used for the simulation. This simulation was applied to prove the validity of the cup structure when attached to the skin as a drug delivery system. When a load of 5 N/m^2 was applied in the direction of the $-z$ axis, the displacement distribution was compared.

■ ASSOCIATED CONTENT

Supporting Information

The Supporting Information is available free of charge at https://pubs.acs.org/doi/10.1021/acsami.1c18750.

Fabrication process of PDMS mold (Figure S1); peel test (Figure S2); structure of the microcup within the self-adhesive microcup patch and images (Figure S3); validation of the structure (Figure S4); application of different types of drugs in the one-cup patch, and actual patch loaded with rhodamine B and SDNA film (Figure S5); real image of the cross section of skin tissue in a region with five cups and picture of the experiment to combine stimulation with ultrasound and an electric current using actual pigskin (Figure S6); and fluorescent and optical images in pigskin of each group for further explanation (Figure S7) (PDF)

■ AUTHOR INFORMATION

Corresponding Author

Jun-Ho Jeong − *Nano-Convergence Mechanical Systems Research Division, Korea Institute of Machinery and Materials, Daejeon 34103, South Korea;* orcid.org/0000-0003-0671-0225; Phone: +82-42-868-7604; Email: jhjeong@kimm.re.kr; Fax: +82-42-868-7123

Authors

Moonjeong Bok − *Nano-Convergence Mechanical Systems Research Division, Korea Institute of Machinery and Materials, Daejeon 34103, South Korea*

Zhi-Jun Zhao − *Nano-Convergence Mechanical Systems Research Division, Korea Institute of Machinery and Materials, Daejeon 34103, South Korea*

Soon Hyoung Hwang − *Nano-Convergence Mechanical Systems Research Division, Korea Institute of Machinery and Materials, Daejeon 34103, South Korea*

Yongrok Jeong − *Nano-Convergence Mechanical Systems Research Division, Korea Institute of Machinery and Materials, Daejeon 34103, South Korea*

Jiwoo Ko − *Nano-Convergence Mechanical Systems Research Division, Korea Institute of Machinery and Materials, Daejeon 34103, South Korea*

Junseong Ahn − *Nano-Convergence Mechanical Systems Research Division, Korea Institute of Machinery and Materials, Daejeon 34103, South Korea;* orcid.org/0000-0002-4090-5440

Ju Ho Lee − *Department of Applied Physics, Dankook University, Yongin 16890, South Korea*

Sohee Jeon − *Nano-Convergence Mechanical Systems Research Division, Korea Institute of Machinery and Materials, Daejeon 34103, South Korea*

Complete contact information is available at: https://pubs.acs.org/10.1021/acsami.1c18750

Notes

The authors declare no competing financial interest.

■ ACKNOWLEDGMENTS

This work was supported by the Center for Advanced Meta-Materials (CAMM), which is funded by the Ministry of Science, ICT and Future Planning, Korea, through the Global Frontier Project (CAMM-No. 2014M3A6B3063707).

■ ABBREVIATIONS USED

SDNA, salmon DNA
FOTCS, trichloro(1*H*,1*H*,2*H*,2*H*-perfluorooctyl)silane
PET, poly(ethylene terephthalate)
PEIE, polyethylenimine

■ REFERENCES

(1) Jeyanathan, M.; Afkhami, S.; Smaill, F.; Miller, M. S.; Lichty, B. D.; Xing, Z. Immunological Considerations For COVID-19 Vaccine Strategies. *Nat. Rev. Immunol.* **2020**, *20*, 615−632.

(2) Poland, E. G.; McGuire, D. K.; Ratishvili, T.; Poland, G. A. The Economics of Global COVID Vaccine Administration during a Pandemic − Why Continue Skin Alcohol Preparation as a Costly but Ineffective Practice? *Vaccine* **2021**, *39*, 1175−1177.
(3) Subbaraman, N. Who Gets a COVID Vaccine First? Access Plans Are Taking Shape. *Nature* **2020**, *585*, 492−493.
(4) van Riel, D.; de Wit, E. Next-Generation Vaccine Platforms for Covid-19. *Nat. Mater.* **2020**, *19*, 810−812.
(5) Zhang, N.-N.; Li, X.-F.; Deng, Y.-Q.; Zhao, H.; Huang, Y.-J.; Yang, G.; Huang, W.-J.; Gao, P.; Zhou, C.; Zhang, R.-R.; Guo, Y.; Sun, S.-H.; Fan, H.; Zu, S.-L.; Chen, Q.; He, Q.; Cao, T.-S.; Huang, X.-Y.; Qiu, H.-Y.; Nie, J.-H.; Jiang, Y.; Yan, H.-Y.; Ye, Q.; Zhong, X.; Xue, X.-L.; Zha, Z.-Y.; Zhou, D.; Yang, X.; Wang, Y.-C.; Ying, B.; Qin, C.-F. A Thermostable MRNA Vaccine against COVID-19. *Cell* **2020**, *182*, 1271−1283.
(6) Wallis, J.; Shenton, D. P.; Carlisle, R. C. Novel Approaches for the Design, Delivery and Administration of Vaccine Technologies. *Clin. Exp. Immunol.* **2019**, *196*, 189−204.
(7) Pollet, J.; Chen, W.-H.; Strych, U. Recombinant Protein Vaccines, a Proven Approach against Coronavirus Pandemics. *Adv. Drug Delivery Rev.* **2021**, *170*, 71−82.
(8) Jenkins, K., II Needle Phobia: A Psychological Perspective. *Br. J. Anaesth.* **2014**, *113*, 4−6.
(9) Prausnitz, M. R.; Mitragotri, S.; Langer, R. Current Status and Future Potential of Transdermal Drug Delivery. *Nat. Rev. Drug Discovery* **2004**, *3*, 115−124.
(10) Paudel, K. S.; Milewski, M.; Swadley, C. L.; Brogden, N. K.; Ghosh, P.; Stinchcomb, A. L. Challenges and Opportunities in Dermal/Transdermal Delivery. *Ther. Delivery* **2010**, *1*, 109−131.
(11) Ganti, S. S.; Bhattaccharjee, S. A.; Murnane, K. S.; Blough, B. E.; Banga, A. K. Formulation and Evaluation of 4-Benzylpiperidine Drug-in-Adhesive Matrix TYPE Transdermal Patch. *Int. J. Pharm.* **2018**, *550*, 71−78.
(12) Al Hanbali, O. A.; Khan, H. M.; Sarfraz, M.; Arafat, M.; Ijaz, S.; Hameed, A. Transdermal Patches: Design and Current Approaches to Painless Drug Delivery. *Acta Pharm.* **2019**, *69*, 197−215.
(13) Alkilani, A.; McCrudden, M. T.; Donnelly, R. Transdermal Drug Delivery: Innovative Pharmaceutical Developments Based on Disruption of the Barrier Properties of the Stratum Corneum. *Pharmaceutics* **2015**, *7*, 438−470.
(14) Lee, Y.; Dugansani, S. R.; Jeon, S. H.; Hwang, S. H.; Kim, J.-H.; Park, S. H.; Jeong, J.-H. Drug-Delivery System Based on Salmon Dna Nano- and Micro-Scale Structures. *Sci. Rep.* **2017**, *7*, No. 9724.
(15) McAlister, E.; Dutton, B.; Vora, L. K.; Zhao, L.; Ripolin, A.; Zahari, D. S.; Quinn, H. L.; Tekko, I. A.; Courtenay, A. J.; Kelly, S. A.; Rodgers, A. M.; Steiner, L.; Levin, G.; Levy-Nissenbaum, E.; Shterman, N.; McCarthy, H. O.; Donnelly, R. F. Microneedle Arrays: Directly Compressed Tablets: A Novel Drug-Containing Reservoir Combined with Hydrogel-Forming Microneedle Arrays for Transdermal Drug Delivery (Adv. Healthcare Mater. 3/2021). *Adv. Healthcare Mater.* **2021**, *10*, No. 2170013.
(16) Bonfante, G.; Lee, H.; Bao, L.; Park, J.; Takama, N.; Kim, B. Comparison of Polymers to Enhance Mechanical Properties of Microneedles for Bio-Medical Applications. *Micro Nano Syst. Lett.* **2020**, *8*, No. 13.
(17) Zhang, X.; Chen, G.; Yu, Y.; Sun, L.; Zhao, Y. Bioinspired Adhesive and Antibacterial Microneedles for Versatile Transdermal Drug Delivery. *Research* **2020**, *2020*, 1−9.
(18) Marjukka Suhonen, T.; Bouwstra, J. A.; Urtti, A. Chemical Enhancement of Percutaneous Absorption in Relation to Stratum Corneum Structural Alterations. *J. Controlled Release* **1999**, *59*, 149−161.
(19) Zorec, B.; Zupančič, Š.; Kristl, J.; Pavšelj, N. Combinations of Nanovesicles and Physical Methods for Enhanced Transdermal Delivery of a Model Hydrophilic Drug. *Eur. J. Pharm. Biopharm.* **2018**, *127*, 387−397.
(20) Shademani, A.; Zhang, H.; Jackson, J. K.; Chiao, M. Active Regulation of on-Demand Drug Delivery by Magnetically Triggerable Microspouters. *Adv. Funct. Mater.* **2017**, *27*, No. 1604558.
(21) Snook, K. A.; Van Ess, R.; Werner, J. R.; Clement, R. S.; Ocon-Grove, O. M.; Dodds, J. W.; Ryan, K. J.; Acosta, E. P.; Zurlo, J. J.; Mulvihill, M. L. Transdermal Delivery of Enfuvirtide in A Porcine Model Using a Low-Frequency, Low-Power Ultrasound Transducer Patch. *Ultrasound Med. Biol.* **2019**, *45*, 513−525.
(22) An, Y.-H.; Lee, J.; Son, D. U.; Kang, D. H.; Park, M. J.; Cho, K. W.; Kim, S.; Kim, S.-H.; Ko, J.; Jang, M.-H.; Lee, J. Y.; Kim, D.-H.; Hwang, N. S. Facilitated Transdermal Drug Delivery Using Nanocarriers-Embedded Electroconductive Hydrogel Coupled with Reverse Electrodialysis-Driven Iontophoresis. *ACS Nano* **2020**, *14*, 4523−4535.
(23) Bok, M.; Zhao, Z.-J.; Jeon, S.; Jeong, J.-H.; Lim, E. Ultrasonically and Iontophoretically Enhanced Drug-Delivery System Based on Dissolving Microneedle Patches. *Sci. Rep.* **2020**, *10*, No. 2027.
(24) Safonov, M.; You, J.; Lee, J.; Safonov, V. L.; Berman, D.; Zhu, D. Hydrogen Generating Patch Improves Skin Cell Viability, Migration Activity, and Collagen Expression. *Eng. Regener.* **2020**, *1*, 1−5.
(25) Wang, Y.; Shang, L.; Chen, G.; Sun, L.; Zhang, X.; Zhao, Y. Bioinspired Structural Color Patch with Anisotropic Surface Adhesion. *Sci. Adv.* **2020**, *6*, No. eaax8258.
(26) Squadrito, F.; Bitto, A.; Irrera, N.; Pizzino, G.; Pallio, G.; Minutoli, L.; Altavilla, D. Pharmacological Activity and Clinical Use of PDRN. *Front. Pharmacol.* **2017**, *8*, No. 224.
(27) Arasu, V.; Dugasani, S. R.; Kesama, M. R.; Chung, H. K.; Park, S. H. Luminophore Configuration and Concentration-Dependent Optoelectronic Characteristics of a Quantum Dot-Embedded DNA Hybrid Thin Film. *Sci. Rep.* **2017**, *7*, No. 11567.
(28) Shin, D. Y.; Park, J.-U.; Choi, M.-H.; Kim, S.; Kim, H.-E.; Jeong, S.-H. Polydeoxyribonucleotide-Delivering Therapeutic Hydrogel for Diabetic Wound Healing. *Sci. Rep.* **2020**, *10*, No. 16811.
(29) Bok, M.; Zhao, Z.-J.; Hwang, S. H.; Kang, H.-J.; Jeon, S.; Ko, J.; Jeong, J.; Song, Y. S.; Lim, E.; Jeong, J.-H. Effective Dispensing Methods for Loading Drugs Only to the Tip of DNA Microneedles. *Pharmaceutics* **2020**, *12*, No. 954.
(30) Baik, S.; Kim, D. W.; Park, Y.; Lee, T.-J.; Ho Bhang, S.; Pang, C. A Wet-Tolerant Adhesive Patch Inspired by Protuberances in Suction Cups of Octopi. *Nature* **2017**, *546*, 396−400.
(31) Baik, S.; Kim, J.; Lee, H. J.; Lee, T. H.; Pang, C. Biomimetic Materials: Highly Adaptable and Biocompatible Octopus-Like Adhesive Patches with Meniscus-Controlled Unfoldable 3D Microtips for Underwater Surface and Hairy Skin. *Adv. Sci.* **2018**, *5*, No. 1870045.
(32) Palchesko, R. N.; Zhang, L.; Sun, Y.; Feinberg, A. W. Development of Polydimethylsiloxane Substrates with Tunable Elastic Modulus to Study Cell Mechanobiology in Muscle and Nerve. *PLoS ONE* **2012**, *7*, No. e51499.
(33) Jeong, S. H.; Zhang, S.; Hjort, K.; Hilborn, J.; Wu, Z. Stretchable Electronic Devices: PDMS-Based Elastomer Tuned Soft, Stretchable, and Sticky for Epidermal Electronics. *Adv. Mater.* **2016**, *28*, 5765.
(34) Wang, Y.; Kohane, D. S. External Triggering and Triggered Targeting Strategies for Drug Delivery. *Nat. Rev. Mater.* **2017**, *2*, No. 17020.
(35) Lakshmanan, S.; Gupta, G. K.; Avci, P.; Chandran, R.; Sadasivam, M.; Jorge, A. E.; Hamblin, M. R. Physical Energy for Drug Delivery; Poration, Concentration and Activation. *Adv. Drug Delivery Rev.* **2014**, *71*, 98−114.
(36) Soto, F.; Jeerapan, I.; Silva-López, C.; Lopez-Ramirez, M. A.; Chai, I.; Xiaolong, L.; Lv, J.; Kurniawan, J. F.; Martin, I.; Chakravarthy, K.; Wang, J. Noninvasive Transdermal Delivery System of Lidocaine Using an Acoustic Droplet-Vaporization Based Wearable Patch. *Small* **2018**, *14*, No. 1803266.
(37) Zhu, W.; Pewin, W.; Wang, C.; Luo, Y.; Gonzalez, G. X.; Mohan, T.; Prausnitz, M. R.; Wang, B. Z. A Boosting Skin Vaccination with Dissolving Microneedle Patch Encapsulating M2e Vaccine Broadens the Protective Efficacy of Conventional Influenza Vaccines. *J. Controlled Release* **2017**, *261*, 1−9.

https://doi.org/10.1021/acsami.1c18750
ACS Appl. Mater. Interfaces 2021, 13, 58220−58228

(38) Ortega-Rivera, O. A.; Shin, M. D.; Chen, A.; Beiss, V.; Moreno-Gonzalez, M. A.; Lopez-Ramirez, M. A.; Reynoso, M.; Wang, H.; Hurst, B. L.; Wang, J.; Pokorski, J. K.; Steinmetz, N. F. Trivalent Subunit Vaccine Candidates for COVID-19 and Their Delivery Devices. *J. Am. Chem. Soc.* **2021**, *143*, 14748−14765.
(39) Jin, X.; Zhu, D. D.; Chen, B. Z.; Ashfaq, M.; Guo, X. D. Insulin Delivery Systems Combined with Microneedle Technology. *Adv. Drug Delivery Rev.* **2018**, *127*, 119−137.
(40) Wang, Z.; Yang, Z.; Jiang, J.; Shi, Z.; Mao, Y.; Qin, N.; Tao, T. H. Silk Microneedle Patch Capable of On-Demand Multi-Drug Delivery to The Brain for Glioblastoma Treatment. *Adv. Mater.* **2021**, No. 2106606.

https://doi.org/10.1021/acsami.1c18750
ACS Appl. Mater. Interfaces 2021, 13, 58220−58228